Multiple-Quantum NMR Studies on Molecular Mixtures

Stefano Caldarelli, Mehdi Yemloul

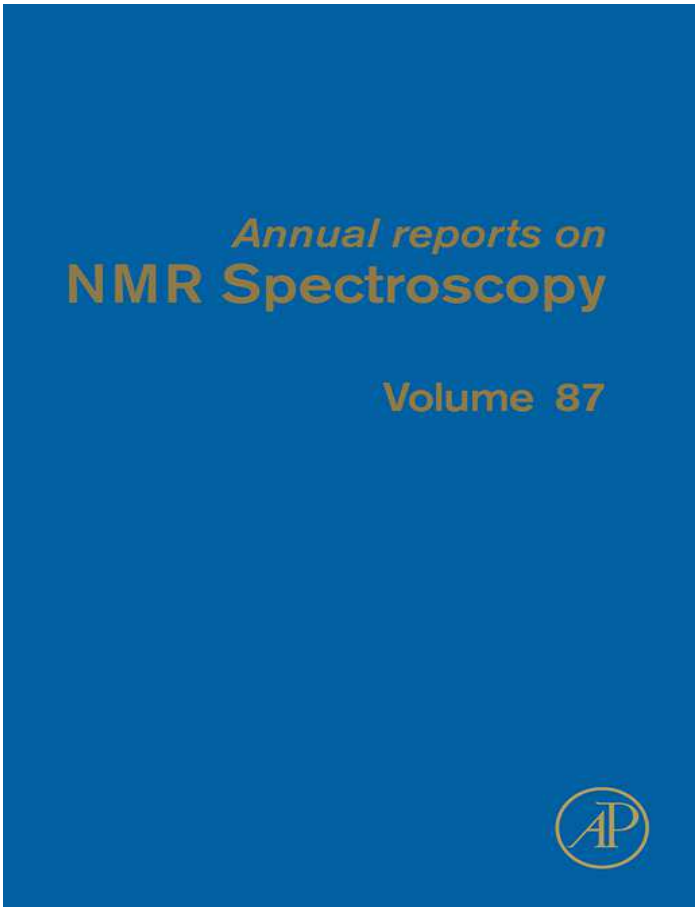

From Stefano Caldarelli and Mehdi Yemloul, Multiple-Quantum NMR Studies on Molecular Mixtures. In: Graham A. Webb, editor, *Annual Reports on NMR Spectroscopy, Vol. 87*, Oxford: Academic Press, 2016, pp. 1-39.
ISBN: 978-0-12-804711-8

Academic Press

CHAPTER ONE

Multiple-Quantum NMR Studies on Molecular Mixtures

Stefano Caldarelli, Mehdi Yemloul
Aix Marseille Université, Centrale Marseille, CNRS, iSm2 UMR 7313, 13397 Marseille, France

Contents

Abstract

Multiple-quantum NMR (MQ-NMR), while being one of the first bidimensional techniques ever experienced, has only recently been adapted to the characterization of complex mixtures of small molecules. This review summarizes recent research that explored this avenue, capitalizing on specific properties of higher order coherences, alone or in conjunction with diffusometry. Finally, we discuss integration of MQ-NMR spectroscopy with modern methods for accelerating the acquisition of multidimensional techniques, showing that, if concentration is appropriate, these experiments can be run in a few seconds.

Key Words: NMR, Mixtures, Metabolites, Natural products multiple quantum

Annual Reports on NMR Spectroscopy, Volume 87
ISSN 0066-4103
http://dx.doi.org/10.1016/bs.arnmr.2015.08.001

1. INTRODUCTION

The detection of multiple-quantum (MQ) coherences is done indirectly, in the easiest setup as a two-dimensional experiment [1,2]. In fact, investigation of MQ coherences excitation, evolution, and reconversion has been the object of many studies already at the inception of multidimensional NMR [3]. Applications have been described to aspects as diverse as simplification of dipolarly coupled proton spectra in liquid crystals, spin counting solids, and simplification of the spectrum of half-integer quadrupolar nuclei. In current days, the most accessed feature of MQ is probably the filtering out of uninformative signals, as in DQF-COSY, or in vehiculating heteronuclear correlations, such as in the HMQC experiment [4].

This review concerns the most recent declination of homonuclear multiple-quantum NMR (MQ-NMR), the analysis of mixtures of small molecules. Since several reviews have been produced over the years covering from the fundamental [5–7] to specific and timely aspects [8,4,9], the interested reader can be find there more detailed discussions on theoretical aspects [10–13]. Nonetheless, some elements of the underlying theory will be provided in order for the reading of this review to be as self-consistent as possible.

2. FUNDAMENTALS OF HOMONUCLEAR MQ-NMR

This section summarizes quickly the basics of MQ-NMR spectroscopy. The richness of the features of the spectra of natural mixtures poses strong challenges to the analytical capabilities of NMR. Besides the difficulties in distinguishing the resonances due to signal overlapping, the situation is further complicated by the large variations in concentration of the components. Adequate techniques to tackle with these issues should provide increased resolution, without losing the capability of annotating the components. MQ-NMR possesses all of these qualities. It naturally reduces the number of resonances by filtering out groups of spins that do not belong to coupled systems of the adequate size. Moreover, increasing the p-quantum order corresponds to a progressive decrease in the peaks in the spectrum (Table 1). Finally, information on the partners of the molecular fragments that host said spin systems is retained in the correlation spectrum. For this reason, MQ-NMR has been reexplored in recent times in the context of the characterization and annotation of multicomponent samples [14–16].

Table 1 Maximum Number of Expected Resonances in Different Spin Systems as a Function of the Observed Coherence Order

	0Q	1Q	2Q	3Q	4Q	5Q
ABC	6	15	6	1		
ABCD	27	56	28	8	1	
ABCDE	110	210	120	45	10	1

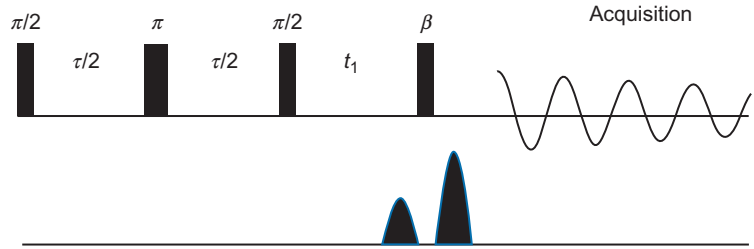

Figure 1 Basic pulse sequence for multiple-quantum filtered (MQF, with t_1 fixed) or MQ correlation spectroscopy using PFG for coherence selection. The value of β and its impact on the spectrum is discussed at several instances in the text.

The simplest approach to exciting MQ coherences in ^{1}H NMR spectroscopy is through direct and indirect couplings. Residual dipolar couplings in liquid crystal solvents were the original source of MQ coherences in the first experiments performed in the late 1970s [17], while J couplings are the commonly used interaction to produce MQ spectra in solution. The first and still most used pulse sequence block employed to this mean is the one represented in Fig. 1.

The first part of which is sometimes referred to as "excitation sandwich," and the delay τ as the "pumping" time. Its action can be depicted as a purely bilinear Hamiltonian [18], acting upon the equilibrium density matrix. For an isolated two-spin AX-coupled system, the relevant term before the second $\pi/2$ pulse is

$$2I_Y^A I_Z^X \sin \pi J\tau \tag{1a}$$

This can be expanded to the highest coherence order, p, for any given spin system to

$$2^p I_{1\phi} \prod_{i=2}^{p} I_Z^i \sin(\pi J_i \tau) \tag{1b}$$

These terms are transformed in mixture of zero- (for even order selection) and MQ coherences by the $\pi/2$ pulse, and the relevant terms are selected by the proper choice of the ratio of the coherence selection gradient pulses.

2.1 Efficiency

Equations (1a) and (1b) illustrate the difficulties that arise if the sample is a mixture of spin systems with different J couplings, which is an occurrence that can already be possible in a single molecule but that becomes very likely in the case of mixtures. This is particularly relevant since typical intensities of multiple-quantum filtered (MQF) spectra can become a couple of order of magnitude less than the regular 1D spectrum (Fig. 2), and thus accessing the maximum efficiency in the MQF process would be an advantage.

The inhomogeneity in intensity produced by a single choice of τ can in principle be compensated if the value of this parameter is allowed to vary along with the t_1 increments if the 2D experiment [19]. If a good guess for the distribution of J couplings exists, a list of τ values can be established. When high-quantum orders are concerned, this approach fails because the small couplings limit the maximum to values of τ that are longer than the relaxation time. In this case, the optimal τ value can correspond to the second smallest J coupling, or to an intermediate value in which the sinusoidal

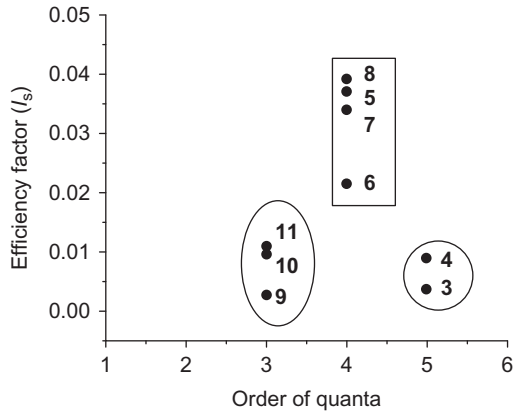

Figure 2 Efficiency of the MQ filtering (MQF) process as a function of the number of quanta, *p*, in the case of a group the aromatic signals of a group of polyphenolics. The values on the ordinates were calculated as the ratio of the integrals in the MQF- and 1Q-spectrum. Note that a variation of a factor of two in the intensity within a MQ Order was observed. *Reprinted with permission from Ref. [14]. Copyright 2010 American Chemical Society.*

oscillations and the exponential relaxation compensate one for the other. An example of this can be seen in Fig. 3, for phenanthrene, representing the evolution of the intensity of a 4-quantum filtered (4QF) spectrum as a function of τ. While the simulations indicated that the optimum intensity should be at around 1 s, as set by $1/2J_{\text{para}}$ for a coupling of 0.5 Hz [20], the experimental maximum signal is found at 320 ms, which corresponds to an effective $1/2J_{\text{ortho}}$ (the reported value being 1.70 and 1.34 Hz) and that is the secondary maximum in the simulation.

Adding more molecules complicates further the choice of the most effective (and minimal) list of τ values. For example, in the case of a mixture of fluorene, anthracene, benz-3,4-pyrene, and 3-aminophenol, one species (anthracene) has a specific coupling pattern and thus presents a maximum excitation of its 4QF spectrum at $\tau = 110$ ms, rather different with respect to other disubstituted aromatic molecules. As a consequence, a 4Q–1Q correlation spectrum cannot be achieved for the said mixture unless the value of 110 ms is not included in the selection of τ values (Figs. 4 and 5).

The obvious trade-off of using a series of τ values is that no value is always optimal for all molecules, and thus, while the spectra become more homogeneous in intensity, sensitivity can be somewhat reduced. This is illustrated in Table 2, in which the nQF signal intensity is compared for a number of systems, for a single or for multiple values of the parameter τ.

An alternative scheme to achieve more homogeneous MQ excitation for multiple spin systems has been proposed, by isotropic mixing, notably using the XY-16 spin-lock scheme [6].

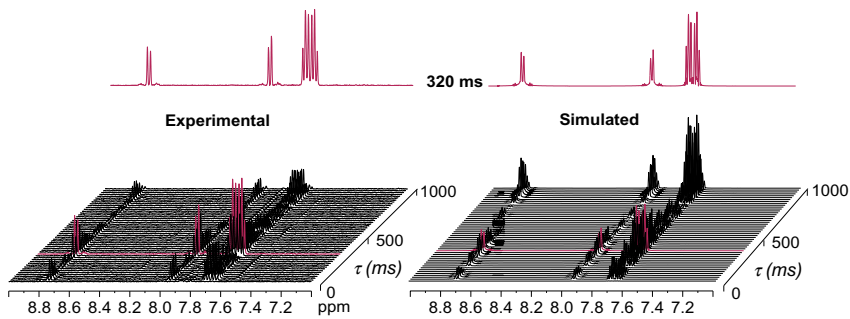

Figure 3 Comparison of experimental (left) and simulated (right) 4QF spectra of phenanthrene, highlighting the effect of relaxation on the choice of the τ value corresponding to the highest intensity (here 320 ms). The simulations were performed using the spin parameters reported in Ref. [17] and neglecting relaxation. *Reproduced from Ref. [19] with permissions from John Wiley and Sons.*

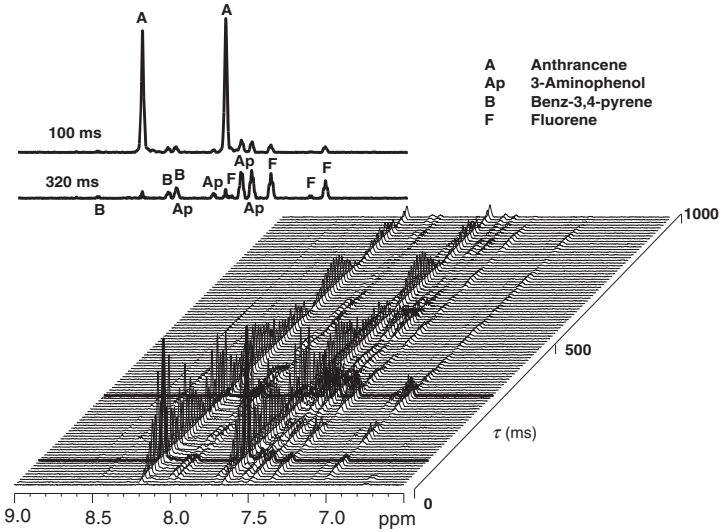

Figure 4 Evolution of the intensity of 4QF signals of a test mixture containing fluorene, anthracene, benz-3,4-pyrene, and 3-aminophenol, as a function of τ. Top: 4QF spectra corresponding to 100 and 320 ms. Bottom: Full evolution of the 4QF signals over the 10–1000 ms range. *Reproduced from Ref. [19] with permissions from John Wiley and Sons.*

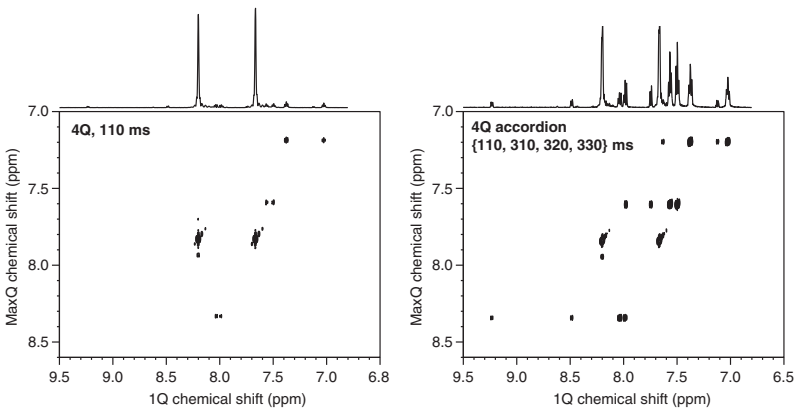

Figure 5 4Q–1Q correlation spectra of the mixture of Fig. 4. The left spectrum was recorded with a single τ value of 110 ms (optimum for anthracene 4QF); the right one was acquired using a sequential variation of the τ value over four vales: 110, 310, 320, and 330 ms. *Reproduced from Ref. [19] with permissions from John Wiley and Sons.*

Table 2 Efficiency of the Single and Multiple τ Multiple-Quantum experiments[a]

		% MQ Efficiency	
Coherence Order	**Molecule**	**Single τ Value**	**Multiple τ Values**
5Q	Benzanilide	*, *, 0.1	0.3, 0.2, 0.1
5Q	*t*-Cinnamic acid	0.6	0.5
4Q	Fluorene	0.3	1.3
4Q	3-Aminophenol	0.2	0.6
4Q	Anthracene	2.6	0.6
4Q	Benz-3,4-pyrene	0.3	0.6
3Q	Acenaphthene	0.4	0.2
3Q	Vanillic acid	0.1	0.2
3Q	1,3,5-Tri-*tert*-butylbenzene	*	0.3

[a]Compared to the single quantum intensity. Asterisks represent spin systems for which negligible intensity was observed.
Reproduced from Ref. [19] with permission from John Wiley and Sons.

2.2 Relay Peaks

It is undeniable that double quantum (DQ) is the most popular MQ coherence found in the literature [8,21,22]. Besides the DQF-COSY experiment mentioned above, several examples of DQ spectroscopy have been reported [6,20]. For the sake of an introduction, we shall thus discuss here the typical aspect of 2Q ^{1}H spectra, which also possess some specific features that can be extrapolated to higher quanta correlations.

Homonuclear DQ correlations became common among spectroscopists thanks to the INADEQUATE experiment for ^{13}C in natural abundance [6]. Here, ^{13}C–^{13}C coupled pairs are selected by the 2Q filter and, due to the statistics of distribution of ^{13}C, they constitute isolate spin systems (i.e., no three-spin coupled system is assumed to exist).

The INADEQUATE plots are of a very intuitive interpretation, since the correlation scheme is between two signals in the 1Q dimension and one in the 2Q axis. This latter can be found at the sum of the chemical shifts of the coupled partners [14].

With respect to its ^{13}C counterpart, ^{1}H–^{1}H DQ spectra may show richer patterns of correlation [16]. More specifically, extra correlation peaks can be found connecting other protons belonging to the same spin system, besides

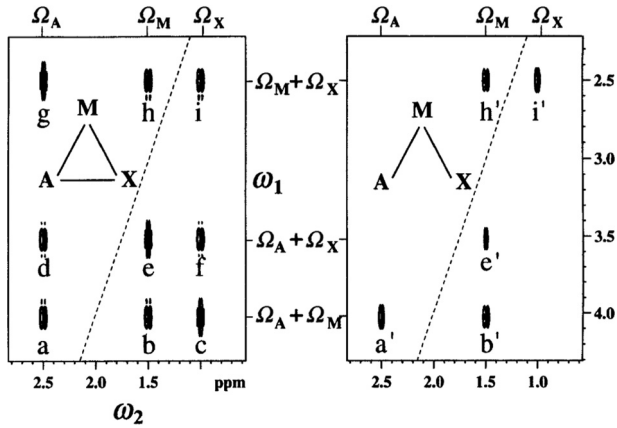

Figure 6 Simulations of ^{1}H DQ correlation spectra for two AMX systems with different *J*-coupling values. Left: $J_{AM}=J_{AX}=J_{MX}=10$ Hz; right: $J_{AM}=J_{MX}=10$ Hz, $J_{AX}=0$ Hz. Chemical shifts were 2.5, 15, and 1.0 ppm in both cases. The relay peaks are the ones not contributing to the sum frequency in the DQ dimension (c, e, g, e′). *From Ref. [23] with permissions from Elsevier.*

the ones the frequencies of which sum up to create the corresponding frequency in the DQ dimension. An example is given in Fig. 6 [23].

The presence of these extra peaks has been considered mainly a nuisance, as they may interfere with the spectral interpretation and reduce the resolution. Accordingly, schemes have been devised to try to minimize their presence, although the efficiency of these filters may vary dramatically with the characteristics of the involved couplings. A strong reduction in the relative intensity of the extra peaks can be achieved by choosing a suitable β tilting angle for the last pulse in the sequence [23]. This issue will be illustrated more in details below in the section dedicated to demonstration of the applications (Fig. 7).

Remote peaks are also present in higher order MQ spectra, but their dependence on the pumping time, τ, and on the β angle has not been completely characterized so far.

2.3 Specificity of the Highest Possible Coherence Order for a Given Spin System

Among all possible *p*-quantum coherences that can be excited, the one corresponding to the highest possible order carries several specificities. As shown in Table 1, it is a singlet, which means that it is not affected by (it commutes with) *J* or dipolar coupling Hamiltonians. The only Hamiltonian influencing this coherence is the sum of the chemical shifts, and thus the

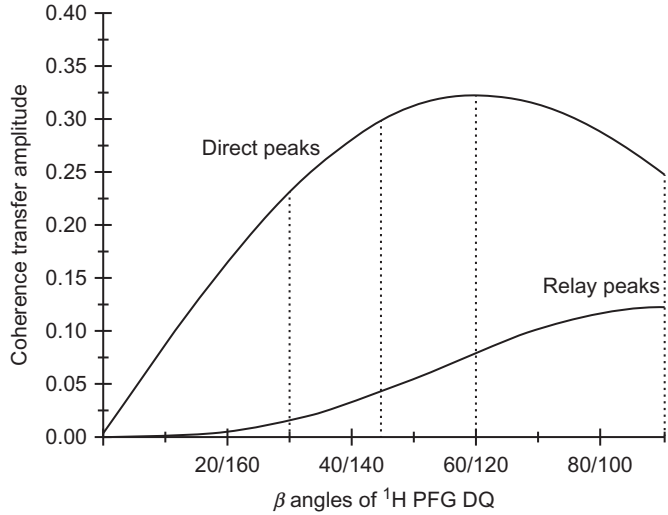

Figure 7 Evolution of the intensity of the direct and relay peaks in echo–antiecho DQ spectroscopy as a function of the tilting angle, β, of the last pulse in the sequence in Fig. 1. *Reprinted from Ref. [23] with permissions from Elsevier.*

singlet is found at the sum of the chemical shifts of the spins that contribute to its creation.

This specific coherence has been dubbed in the past total spin coherence [24] or, perhaps somewhat more explicitly, Maximum-Quantum (MaxQ) order [14]. In the seminal paper by Garbow *et al.* [25], this particular coherence order has been very well described.

It commutes with all terms in the Hamiltonians, with the exception of the sum of the chemical shifts, as that it is a singlet, but it can also be used to counter the effects of field homogeneity (as shown in Fig. 8).

Interestingly, this property of the MaxQ order has not been exploited much [26], since a similar effect can be achieved otherwise and with a much reduced signal losses, by zero-quantum filtering, demonstrated in the case of mixtures in heterogeneous phases, such as tissues, as a possible alternative (or complement) to high-resolution magic-angle-spinning (HR-MAS) [27].

3. MQ SPECTROSCOPY FOR MIXTURE ANALYSIS

3.1 DQS Analysis of Mixtures

Dalvit *et al.* [28] revisited this particular coherence order for the simplification of the spectra of mixtures. While DQ-^{1}H spectroscopy shares all the issues related to intensity dependence on the τ parameter, one of its main

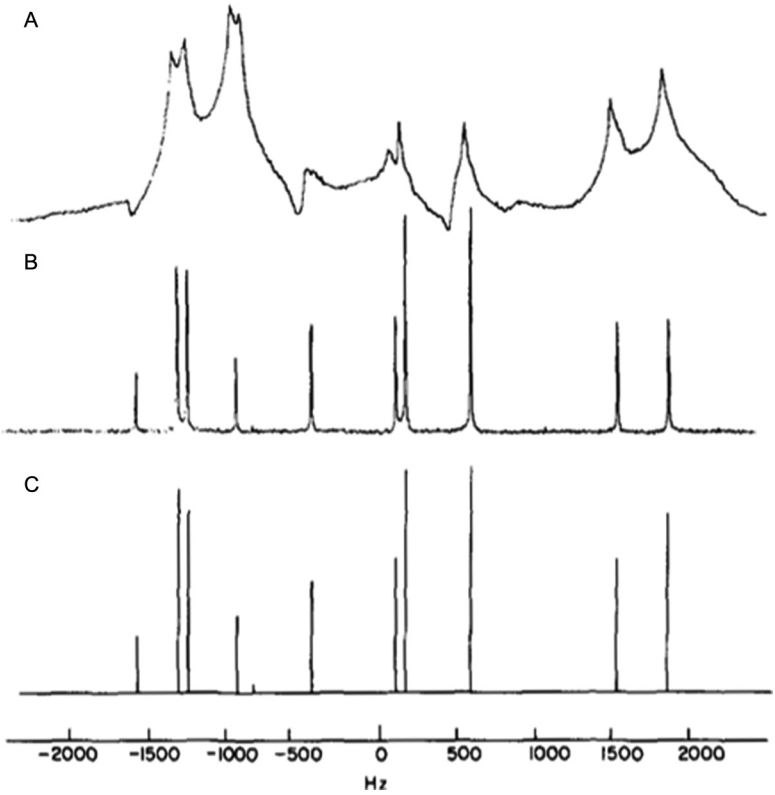

Figure 8 Original demonstration of the line-narrowing effects of the MaxQ coherence order in acquired in a highly inhomogeneous magnetic field. (A) ^{1}H 1Q spectrum of acetaldehyde dissolved in the nematic liquid crystal Eastman 15320 in the presence of a gradient of magnetic field; (B) 1Q trace of the MaxQ–1Q correlation of the same sample and in the same conditions as in (A); (C) simulation spectrum of acetaldehyde. *Reproduced from Ref. [25] with permissions from the American Institute of Physics.*

assets is that it provides a spectrum tantamount to COSY but without the nuisances linked to the presence of diagonal peaks. If the relay peaks are neglected as a first approximation (they will be discussed more in details below), indeed the peaks that can be observed in a DQ spectrum corresponds to the pairwise correlation through J coupling, which is the same information observed in COSY layouts. While introducing the interest of DQF-COSY, the difficulty of determining cross-peaks close to the diagonal was pointed out as a major drawback of COSY spectra. This issue is even more pronounced for mixtures, where the range of concentrations of the components can be spanning a couple of order of magnitudes for typical

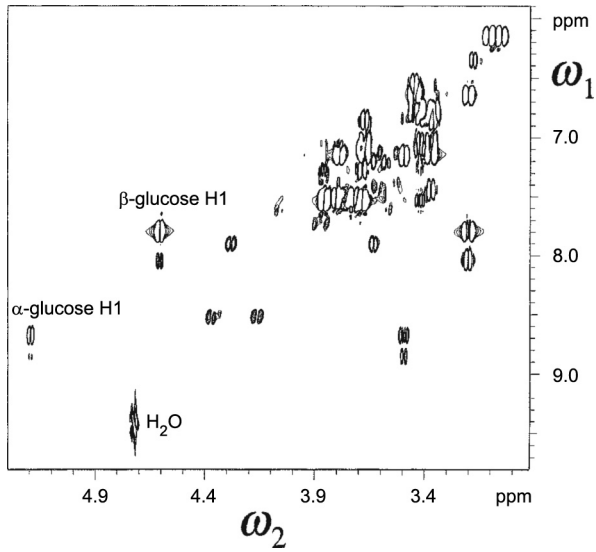

Figure 9 Demonstration of DQ correlation spectroscopy on a mixture of a sample of plasma from rat. An expanded region containing the spin systems of glucose and the residual H_2O signal is shown. *Reproduced from Ref. [28] with permissions from John Wiley and Sons.*

cases viable for NMR analysis. The example of glucose in serum analysis is poignant, as its signal, in the mM range, tends to obscure other peaks in the same region (Fig. 9).

The quantitative aspects of DQ NMR spectroscopy were investigated for mixtures recently [29] and subsequently applied on extracts of breast cancer cell lines (Fig. 10) using the spiking approach. This allowed to determine with high accuracy the variations of concentration of 15 targeted metabolites (Fig. 11).

The observed variations of the metabolite concentrations along the three series of extracts allowed a clear discrimination, as depicted in the corresponding principal component analysis plot (Fig. 12).

3.2 The MaxQ Approach

As mentioned in Section 1 (Table 1), the simplest MQ spectrum is associated to the coherence order, p, which is equal to the number of coupled protons, and the spectrum of which is a simple singlet. The shape of the MaxQ signal has particular interest in the identification of compounds in mixture with strongly overlapping spectra. Here, the 2D correlation allows unraveling the spectrum of the single spin systems as the traces along the MaxQ

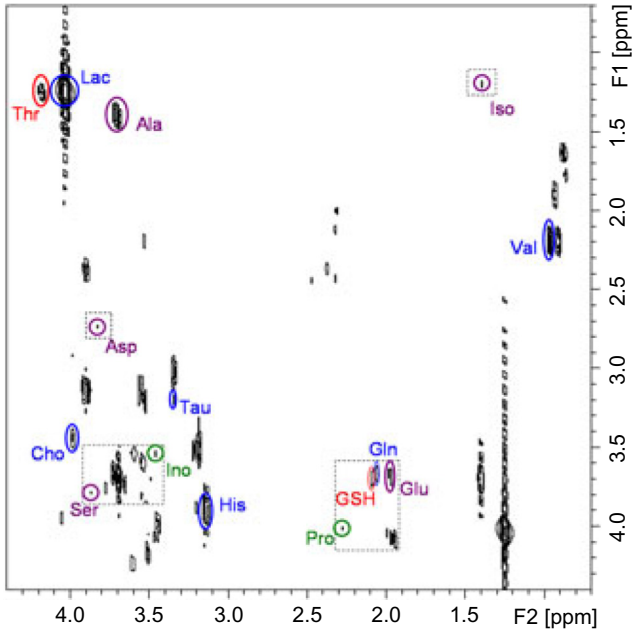

Figure 10 ^{1}H DQS spectrum of an extract of a breast cancer cell line, showing the easy determination of several metabolites %. *Reproduced from Ref. [29] with permission from John Wiley & Sons, Ltd.*

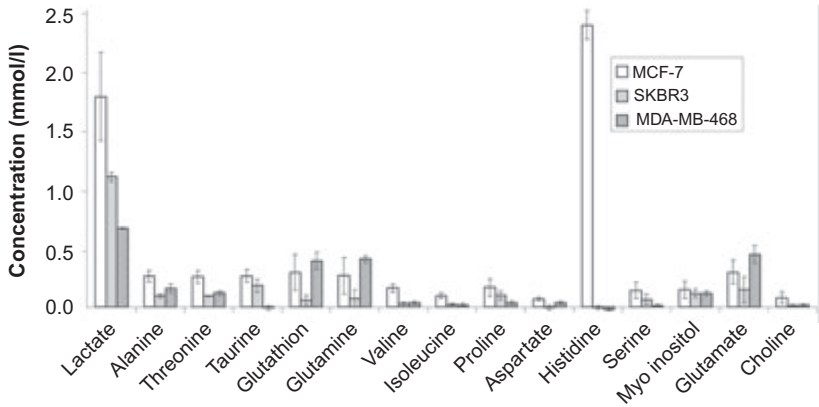

Figure 11 Metabolites quantified through 2Q ^{1}H NMR (as shown in Fig. 10), using the spiking method, from three different breast cancer cell lines %. *Reproduced from Ref. [29] with permission from John Wiley & Sons, Ltd.*

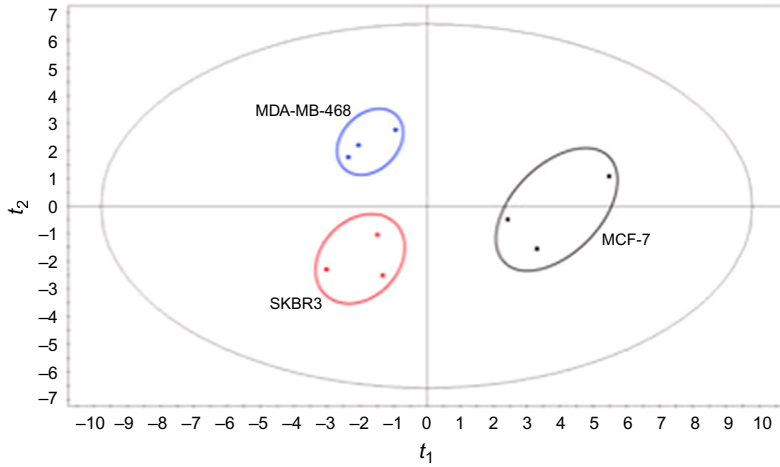

Figure 12 Principal component analysis on the concentrations of 15 target metabolites from extracts from three breast cancer cell lines, showing the excellent differentiation of the three samples achieved by DQS. The first-principal component (t_1) accounted for 59% of the variance, while the second one (t_2) for 27%. *Reproduced from Ref. [29] with permission from John Wiley & Sons, Ltd.*

dimension of the corresponding singlets, much in the spirit of other analytical approaches, for instance based on chromatography. It should be noted that the excitation of the highest possible quantum order in small molecules has been also revived by Suryaprakash and coworker [30], in the context of spin-state selective analysis for heteronuclear spectroscopy.

The first proof of principle of analytical MaxQ spectroscopy was provided by testing its resolving power on a mixture of 11 aromatic compounds: naphthalene, anthracene, phenanthrene, fluoranthene, triphenylene, *o*-terphenyl, phenol, acetanilide, benzophenone, biphenyl, and dibenzyl, the structures of which are depicted in Fig. 13. In accordance with the analysis of the composition of the molecular fragments in the analyzed mixture, the maximum accessible quantum order here is equal to 5.

The analytical challenge here comes from the little differences in the spectra for the 28 distinguishable chemical shifts in the aromatic region, which spans a small spectral window of less than 2 ppm, as illustrated in the corresponding spectrum (Fig. 13). Inspection of the molecular structures reveals that the maximum number of coupled spins here is 5, for monosubstituted aromatics. The series of pQ–1Q correlation spectra, with $p = 1$–5, is shown in Fig. 14. Note that the progressive rarefaction of the signals with increasing p is due here to two concurrent phenomena: on one

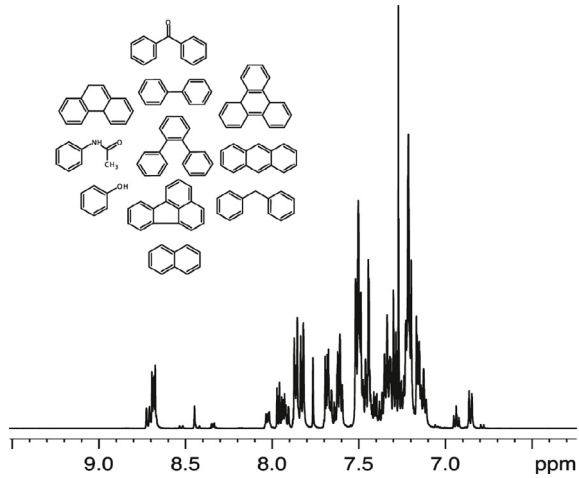

Figure 13 ^{1}H NMR spectrum of 11 aromatic molecules test mixture, the structure of which is represented in the inset. *Reproduced with permissions from Ref. [14]. Copyright 2010 American Chemical Society.*

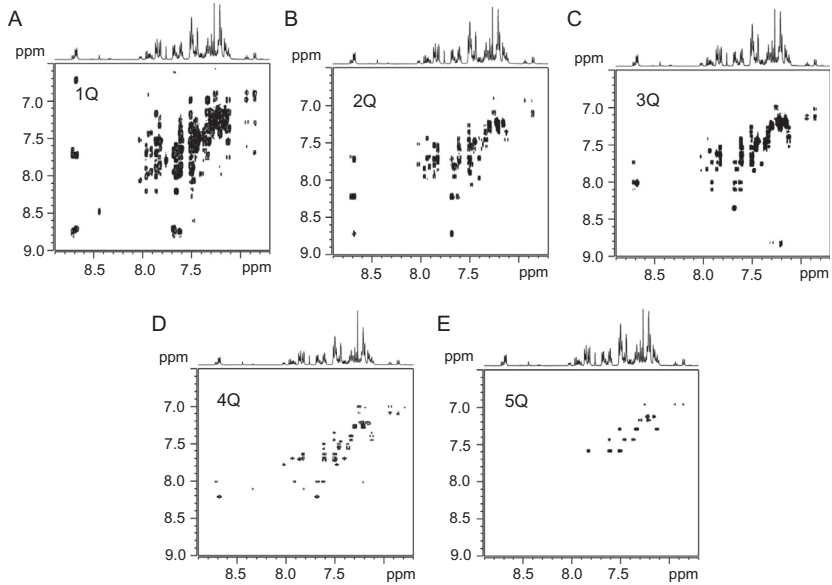

Figure 14 Series of *p*Q–1Q correlation spectra ($p = 1$–5, A–E) for the mixture depicted in Fig. 13. *Reproduced with permission from Ref. [14]. Copyright 2010 American Chemical Society.*

hand, only the spin systems with at least *p*-coupled protons survive in the 1Q dimension (*p*Q filtering); and then the surviving MQ signals have a reduced fine structure, as explained above (Table 1). The spectra were traced with units in the MQ dimension scaled by the coherence order,

$$\delta^{R}_{\mathrm{MaxQ}} = \sum_{i=1}^{p} \frac{\delta_{i1\mathrm{Q}}}{p} \tag{2}$$

which allows an easier comparison among the MQ orders.

The MaxQ layout is best recognizable in the 5Q spectrum for the six monosubstituted molecules of the set (Fig. 15A). For annotation, the multiplet structure and the chemical shift of the individual molecules can be extracted from the individual traces, as shown in Fig. 15B.

Lowering the *p*-order by one unit (Fig. 16) reveals two different kinds of cross-peaks: five more MaxQ ones (i.e., singlets), along with more complex ones. Indeed, the peaks in the 4Q correlation spectrum stems from molecular fragments with either four or five protons. These latter produce non-MaxQ signals, identifiable because they concern spin systems already seen in the 5Q spectrum. For this particular ensemble, the combination of the 4Q and 5Q spectra is sufficient for detecting all molecules, although complete annotation of the spin systems requires recording the 3Q and 2Q spectra as well.

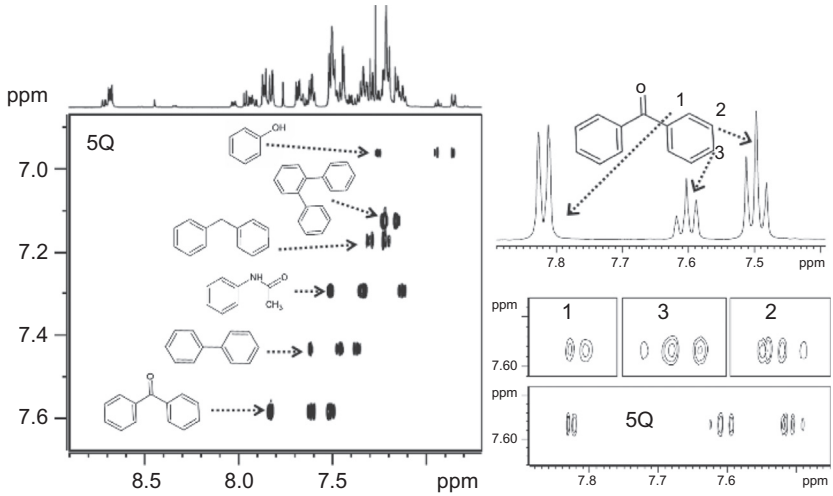

Figure 15 (A) 5Q correlation spectrum. (B) Trace corresponding to the 7.6 ppm δ_{MaxQ} and details, with an expansion of the same peak in the 5Q correlation plot. *Reproduced with permission from Ref. [14]. Copyright 2010 American Chemical Society.*

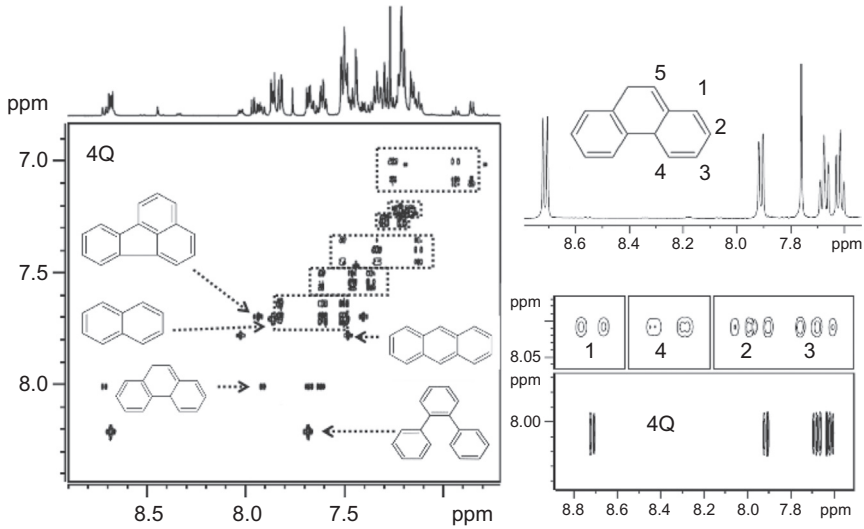

Figure 16 4Q correlation spectrum of the mixture of poly- and monoaromatic compounds depicted in Fig. 13, allowing the identification of six spin systems. A weak signal at $\delta_{MaxQ} = 8.1$ ppm, corresponding to triphenylene, has not been drawn in order not to overcharge the figure. *Reproduced with permission from Ref. [14]. Copyright 2010 American Chemical Society.*

4. ANALYTICAL APPLICATIONS OF THE MaxQ PRINCIPLE

4.1 Characterization of Polyphenolics in Natural Substances

Polyphenolics are molecules with strong biological activity, particularly as antioxidants [31–35]. They are commonly found in many products of natural origin, and they exist in such a variety of forms that they present a challenge to the analyst [36–38]. Therefore, MaxQ NMR was tested as a possible addition to the analytical toolbox for these molecules.

First, a standard sets used to evaluate phenolics separation in liquid chromatography was investigated. All molecules could be identified, using from one to five quanta coherences [15]. The observed overall excitation–reconversion efficiency, using a single τ value, was found to be around 0.3–4% in this case (Fig. 2 referred to this sample).

Next, the MaxQ strategy was tested for a qualitative characterization of the polar extract of a commercial extra virgin olive oil, the aromatic region of which is also expected to be essentially constituted by polyphenolics.

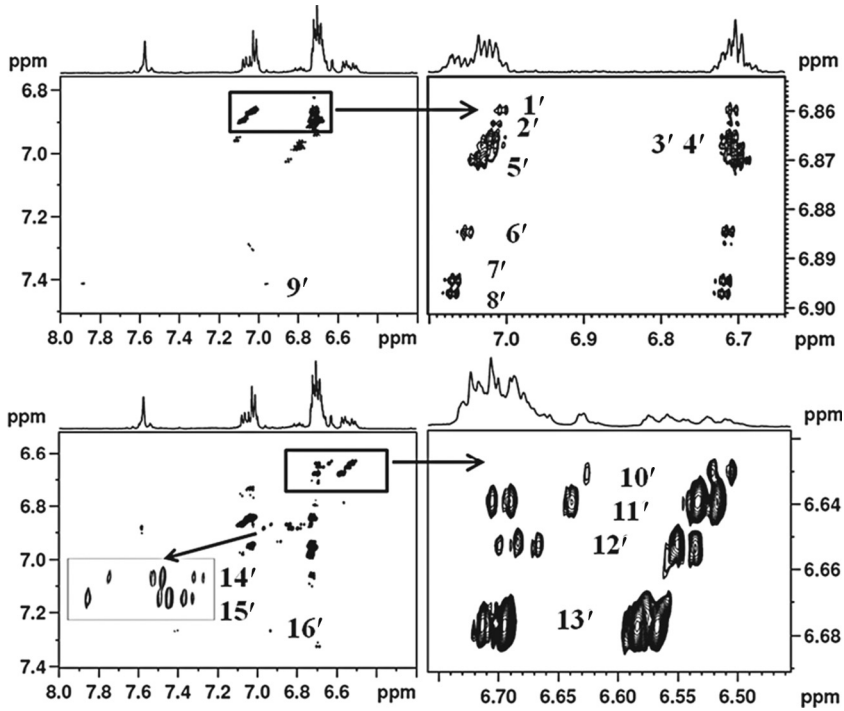

Figure 17 4Q (top) and 3Q (bottom) correlation spectra of a polar extract of an extra virgin olive oil. Spectra on the right correspond to selective experiments performed on the regions boxed in the spectra on the left. See text for a discussion. *Reproduced from Ref. [15] with permission from The Royal Society of Chemistry.*

No signal was found in the 5Q spectrum. The 4Q spectrum (Fig. 17, top) revealed one well-isolated peak (labeled 9′), and a cluster of overlapping signal, in the region 6.85–6.90 ppm for δ_{MaxQ}. A second experiment, conducted with selective excitation of this crowded section of the spectrum, produced an increased resolution, allowing to detect at least five molecules in the area of most intense overlapping, plus three more nearby. Altogether, the 4Q spectrum allowed separation of nine signals, although it is possible that the highly overlapping region (at a δ_{MaxQ} of about 6.865 ppm) could be resolved further by more selective experiments. The annotation, obtained by comparison with the literature [15], is shown in Table 3.

4.2 Quantitative Analysis Using MaxQ Spectroscopy

Although quantitative NMR is so developed that it can be considered as a field on its own, the vast majority concerns 1D ^{1}H spectroscopy [39,40]. In fact, the introduction of common 2D experiments as tools for quantitation

Table 3 Annotation of the Polyphenolics Molecules in the Polar Extract of an Extra Virgin Olive Oil, as Determined Through MaxQ Experiments

Phenolic Fraction of an Extra Virgin Olive Oil

No.	Molecule (MaxQ)	δ_{MaxQ} (ppm)
1′	Ligstroside aglycon (4Q)	6.860
2′	–	6.863
3′	–	6.865
4′	–	6.867
5′	Dialdehydic form of ligstroside lacking the carboxymethyl group (4Q)	6.870
6′	Tyrosol (4Q)	6.885
7′	Tyrosol acetate (4Q)	6.894
8′	Aldehydic form of ligstroside (4Q)	6.897
9′	Apigenin (4Q)	7.42
10′	Oleuropein aglycon (3Q)	6.63
11′	Hydroxytyrosol (3Q)	6.64
12′	Aldehydic form of oleuropein (3Q)	6.65
13′	Hydroxytyrosol acetate (3Q)	6.68
14′	Pinoresinol (3Q)	6.84
15′	Acetoxy pinoresinol (3Q)	6.88
16′	Luteolin (3Q)	7.27

MaxQ order of detection is indicated in parenthesis.
Adapted from Ref. [15] with permission from The Royal Society of Chemistry.

of mixtures has been delayed by issues such as the duration of the experiment [41–62]. Indeed, only in recent years, the question has begun to be investigated, and MQ-NMR was among the first techniques to be explored to this respect.

The key point in the use of *n*D NMR for quantitation is that the intensity of the cross and diagonal peaks depends linearly on the concentration of the analyte, but also uniquely on the transfer function, that describes the efficiency of the underlying coherence transfer processes.

Thus, the peak intensity in a 2D MaxQ spectrum, as function of the concentration of the analyte C, can be expressed as

$$I_{\mathrm{MaxQ}} = Kf(\tau, \{J\})C \tag{3}$$

where K is a proportionality constant, f is the transfer function linked to the pulse sequence used here, and $\{J\}$ indicates the specificity of the J-coupling network under scrutiny.

In principle, the factor f can be calculated from first principles if the characteristics of the spin system, including relaxation rates, are perfectly known. In practice, this is not a viable option, particularly if dealing with mixtures of unknown composition. This is also an issue for high pQ spectra, since, as discussed above, their intensity depends strongly on the smaller J couplings, which are the most difficult to measure accurately. In this case, a calibration curve, or the spiking method as seen above for DQ spectroscopy, is still the best options. An advantage of the MaxQ layout is that its projection along the indirect dimension is very simple and can be compared to chromatograms. If the MQ spectrum consists only of MaxQ signals, the quantitative analysis can be therefore limited only to the projection along the indirect dimension. Otherwise, the most general approach consists in measuring the cross-peak intensities (or volumes, if different line widths are expected) in the pQ spectrum.

Both approaches were tested on the 16 polycyclic aromatic hydrocarbons (PAHs) declared priority pollutants listed by the EPA, the concentration of which was made vary in between 0.25 and 4 mM. The two methods provided very good overall accuracy (Fig. 18 and Table 4).

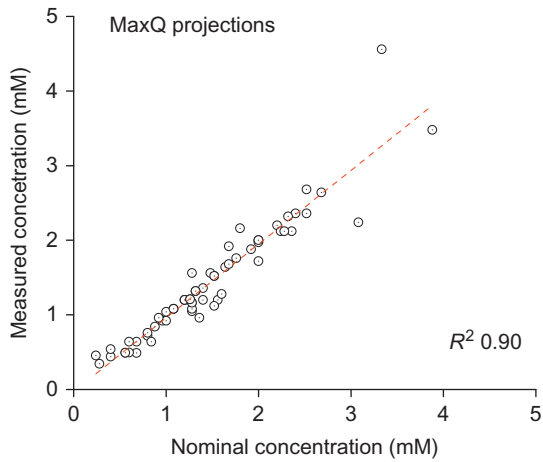

Figure 18 Evaluation of the linearity of MaxQ spectroscopy on the determination of 16 polycyclic aromatic compounds (PAHs). See text for details. *Reproduced from Ref. [16] with permission from The Royal Society of Chemistry.*

Table 4 MaxQ NMR Quantitative Analysis of the EPA 16 Priority PAH Pollutants

No.	Analyte	Average δ^{R}_{MaxQ} (*n*Q in ppm)[a]	$\Delta\delta^{R}_{MaxQ}$ (ppm)[b]	Weight of the Analyte in 500 µl of Solvent (µg)	R^2 of the Concentration Calculated by Deconvolution of the MaxQ Projections	R^2 of the Concentration Calculated by Integration of the MaxQ Traces
1.	Fluorene	7.574 (4Q)	0.024	50–200	0.975	0.990
2.	Fluoranthene	8.108 (3Q), 7.712 (4Q)	0.034	100–250	0.948	0.975
3.	Naphthalene	7.720 (4Q)	0.001	25–250	0.905	0.948
4.	Benzo[*b*] fluoranthene	7.850 (3Q), 7.760 (4Q), 8.051 (4Q)	0.001, 0.005	75–225	0.878	0.914
5.	Benzo[*k*] fluoranthene	8.076 (3Q), 7.785 (4Q)	0.002	75–200	0.934	0.990
6.	Anthracene	7.791 (4Q)	0.001	125–250	0.957	0.941
7.	Indeno[123*cd*] pyrene	8.230 (3Q), 7.841 (4Q)	0.002	75–225	0.970	0.984
8.	Phenanthrene	8.011 (4Q)	0.001	25–70	0.973	0.982
9.	Benzo[*a*] anthracene	7.880 (4Q), 8.039 (4Q)	0.001, 0.004	100–225	0.985	0.929
10.	Chrysene	8.081 (4Q), 8.415 (4Q)	0.002	100–250	0.994	0.953

11.	Dibenzo[*a*,*h*] anthracene	8.089 (4Q)	0.003	75–225	0.931	0.985
12.	Benzo[*a*]pyrene	8.004 (3Q),[c] 8.280 (4Q)	0.002	50–225	0.977	0.982
13.	Acenaphthene	7.491 (3Q)	0.01	125–225	0.950	0.945
14.	Acenaphthylene	7.679 (3Q)	0.000	50–200	0.993	0.982
15.	Pyrene	8.133 (3Q)	0.000	25–225	0.886	0.980
16.	Benzo[*ghi*] perylene	8.427 (3Q)	0.000	125–250	0.965	0.913

[a]Average value observed over the five mixtures analyzed.
[b]Maximum spread observed.
[c]Not observed, calculated based on 1Q chemical shift.
Reproduced from Ref. [16] with permission from The Royal Society of Chemistry.

The accuracy of 1D ^{1}H qNMR has been determined to be linked, not surprisingly, to the signal-to-noise ratio (technically the peak to signal-to-noise ratio, PSNR), with the error on the measurement becoming appreciably high for PSNR of the order of 10 or less [45]. Thus, the sensitivity of a given 2D method is important not only to determine its detection limit but also to estimate its accuracy. Lack of sensitivity is a common drawback in NMR, which has been addressed either by increasing the magnetic field or by enhancing the weak nuclear magnetic polarization. Methods addressing this last avenue, however, remain quite system specific and are likely to introduce some bias in the analysis of unknown mixtures, particularly the ones of natural origin. Thus, for the time being, sensitivity enhancement for mixtures is best obtained by taking the analysis to higher fields. The downside of increasing the proton reference frequency, however, is that constant resolution can only be achieved at the expenses of longer experiments. The trade-off is still in favor of high field, but it is best assessed phenomenologically. Figure 19 shows that detection with very good PSNR values can be achieved in 24 h for the 4Q spectrum of the mixture of 16 PAHs, for an equimolar concentration of 30 μM.

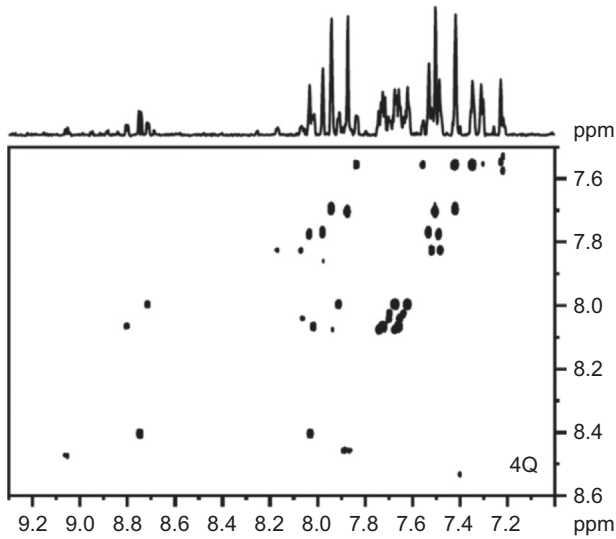

Figure 19 4Q–1Q NMR correlation spectrum recorded at high field (1000 MHz ^{1}H frequency) on a cryogenic probe, for testing of the sensitivity limit of the method (1 day of acquisition time). The concentration of each fragment in the test mixture was of 30 μM. *Reproduced from Ref. [16].*

5. ACCELERATION OF MQ EXPERIMENTS

The advent of *n*D NMR experiments in the analysis of mixtures has been hold off, among other things, by the long experimental times usually associated to these techniques if sufficient resolution is requested in the indirect dimension(s). This point is particularly relevant if the analysis concerns a series of samples, as in metabolomics studies. Recently, a few possibilities have been introduced and discussed that achieve sensible acceleration of the experimental times required to obtain a *n*D spectrum well resolved along all dimensions [46–49].

5.1 Ultrafast DQ Spectroscopy

One of these approaches, ultrafast (UF) NMR, has been demonstrated in the case of DQ spectroscopy [50]. The principle of UF NMR has been reviewed a few times, and thus here we shall only outline quickly its principle of functioning, along with the main advantages and limitations. Inspired by a very popular approach in IRM, echo planar imaging, UF NMR aims at reintroducing the multiplexing power of Fourier analysis in all dimensions of an *n*D NMR experiment. This is in contrast with the classic way of performing 2D NMR, where the "indirect" dimension, that is to say not directly acquired by the receiver coil, is sampled one point at the time by increasing sequentially a time parameter. In UF NMR, the indirect dimension is coded in one step, using a pulse field gradient (PFG) to encode a position dependency upon the spins and using frequency-swept excitation pulses.

The exposed limit in overall matrix size resolution of UF NMR can be partially overcome if more than one scan is employed to record the spectra. In this case, interleaved acquisition is possible. This scheme consists at shifting the second acquisition in time so that the k/t space is sampled on a finer grid. For instance, in this case, an interleaved factor of 4 was used that was used to provide an augmentation of the resolution by a factor of two in both dimensions.

It should be noted that an alternative to interleaved acquisition for increasing the resolution in UF NMR has also been proposed, based on nonlinear sampling of the time domain dimension [51]. The pulse sequence used for UF DQ NMR is shown in Fig. 20A, which is a simple modification of the published UF COSY [52] sequence with the addition of the pumping

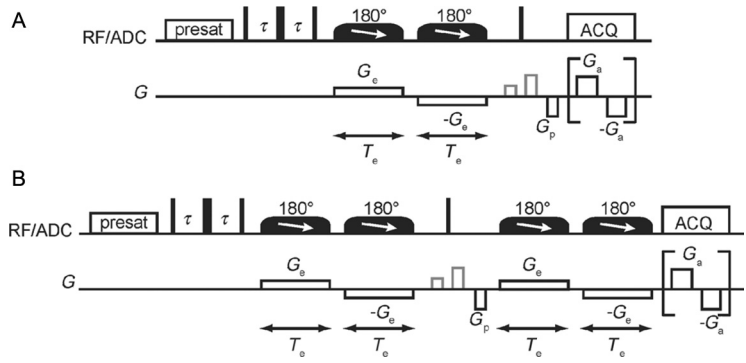

Figure 20 Pulse sequences for UF DQ spectroscopy. (A) The UF version of the pulse sequence shown in Fig. 1. (B) Modified sequence to provide spectra symmetric around the diagonal rather than at the double-quantum frequency. *Reprinted from Ref. [50] with permission from The Royal Society of Chemistry.*

sandwich. A modified version that provides spectra with cross-peaks in the same position as in the equivalent COSY plot is shown in Fig. 20B.

UF NMR was applied to DQ NMR, using this interleaved approach, with a factor of 4, on a 600 MHz spectrometer equipped with a cryoprobe. The results are shown in Fig. 21. The last pulse β has a duration corresponding to a 120° flip angle, in order to minimize the ratio direct/relay peak. Note that this step is really not a strictly bonding condition, as the presence of a relay peak confirms the presence of a spin system and provides further indications on its partnership. In a way, relay peaks can be seen, in terms of information on the composition of a mixture, as a partial of a TOCSY pattern. Although all information is available in the 2Q–1Q correlation layout, sometimes it may be convenient to translate this plot into one resembling more closely the cross-peak disposition as observed in COSY. This could be just for the sake of visual comparison or for searching databases, which generally do not carry any 2Q information. This result can be obtained by a simple shearing transformation (Fig. 22B) or by applying a pulse sequence that refocuses the 2Q coherence into 1Q before acquisition [53,54]. This is shown in Fig. 22C for a single molecule in solution, sucrose. Carbohydrates are often among the most difficult systems to characterize by NMR, as most of their resonances fall in a narrow spectral region, for once, and cross- and diagonal peaks consequently overlap. Moreover, the signal of carbohydrates is ubiquitous in biofluids, and it may blank other less concentrated components. DQ spectroscopy simplifies the *J*-coupling correlation spectrum of sucrose considerably, as can be best exemplified in the area

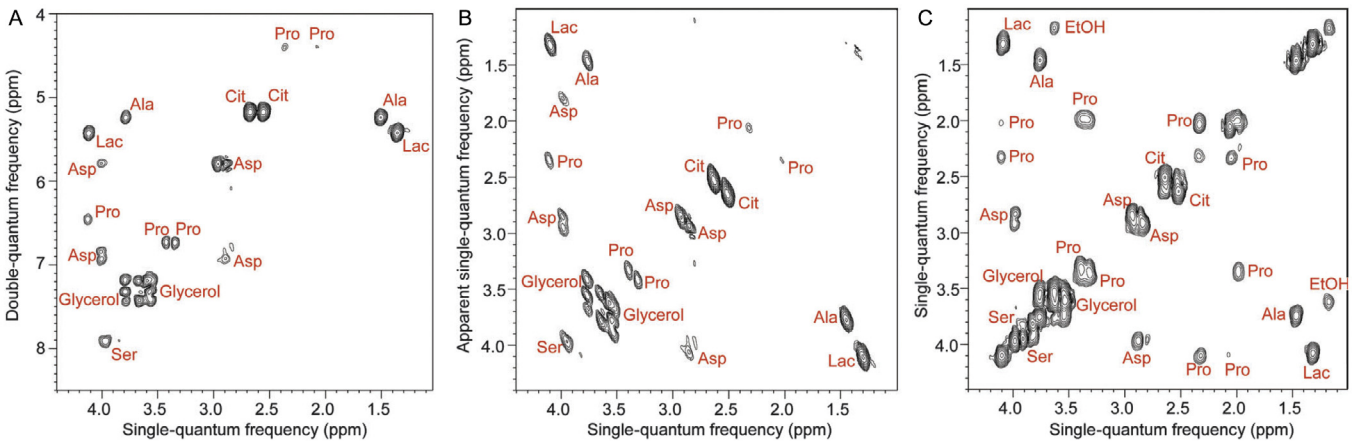

Figure 21 Ultrafast NMR spectra of a mixture of seven metabolites in H_2O/D_2O (90/10): (A) DQS; (C) COSY. Spectrum (B) was obtained from spectrum (A) by a shearing transformation at a processing stage. *Reprinted from Ref. [50] with permission from The Royal Society of Chemistry.*

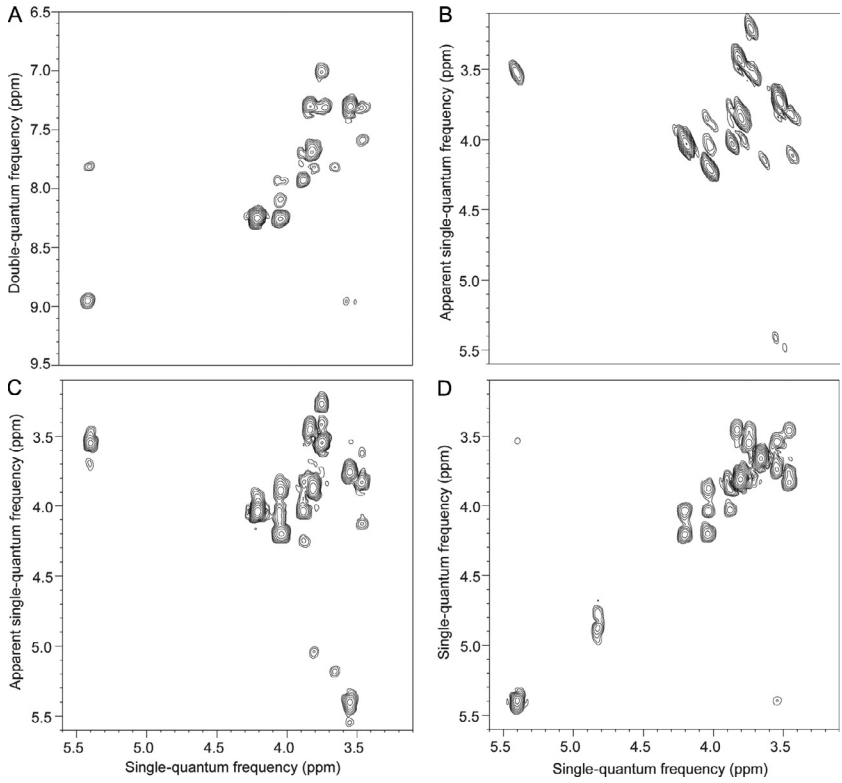

Figure 22 Ultrafast NMR spectra of 0.1 M sucrose in D_2O: (A) DQS (sequence shown in Fig. 20A); (C) DQSsy (sequence shown in Fig. 20B); (D) COSY. Spectrum (B) was obtained from spectrum (A) by a shearing transformation at a processing stage. *Reprinted from Ref. [50] with permission from The Royal Society of Chemistry.*

around 3.5–3.7 ppm comparing the UFCOSY spectrum (Fig. 22D) and the DQ counterparts.

The UF DQS was demonstrated on a synthetic mixture of common metabolites, in a relatively high concentration from 13 to 27 mM. However, alternative approaches that consist of averaging multiple spatially encoded spectra [55] have been successfully used on quantitative NMR and metabolomics [56], where samples are much less concentrated and can have a large dynamic range of concentration [51]. Again the use of four interleaved acquisition in the MQ implementation of UF spectroscopy allowed the analysis of the spectral region that carries most of the information, in between 1 and 4.5 ppm in the 1Q dimension. All peaks could be detected, although no optimization for optimal and homogeneous MQ excitation was

performed. Some relay peaks are visible, although just in a few cases, due to the choice of 120° tilting angle for the reading pulse, which is indeed meant to favor the direct connectivity peaks.

While these extra signals contribute to enhancing the signal crowding, with possible loss of resolution, it should be noted that they could be extremely useful in the case of mixture to properly annotate spin systems, much in the way as TOCSY is the standard tool in mixture analysis rather than the less complete COSY that only provides partial connectivity.

The acquisition of ultrafast 2D spectra of semisolid samples, with a HR-MAS setup, was also recently demonstrated [57]. This approach is perfectly compatible with high-throughput studies or the analysis of fragile samples. In this case, the synchronization of the detection and the rotor period is crucial to avoid the destructive interferences occurring due to the misalignment of the magnetic field gradient axis and of the rotor [58]. Despite the precautions, replicas of some of the peaks are observed in the UFCOSY spectra, thereby increasing the complexity of the spectra. Therefore, the UF DQS is especially useful with the HR-MAS system, as it makes it possible to remove the uninformative autocorrelation peaks, and the associated images [50].

One of the important limitations concerns the spectral width that can be covered in a single scan. This is directly related to the nominal maximum gradient intensity for HR-MAS probe (54 G/cm). The interleaved approach allowed to explore the spectral width of 1.07 and 2.12 ppm in the conventional and the ultrafast dimension, respectively, and the usual processing strategies for ultrafast NMR spectra allowed to obtain, on a standard HR-MAS setup, high-quality UF DQS spectra in 6 s.

5.2 Nonuniform Sampling

A second approach to compressing the experimental time of *n*D eNMR experiments relies on nonuniform sampling (NUS) of the grid corresponding to the time signal [59,60]. In short, fast Fourier transform algorithms exploit a regularity in the sampling along each of the *n* dimensions of interest, the dwell times, DW. This is in turn determined by the Nyquist theorem, to be the reciprocal of the spectral width. The number of points, TD, acquired in each time domain is conversely determined by the desired resolution, which is a function of the total time of acquisition, and thus to TD × DW. In a typical *n*D experiment, however, the number of points in the frequency domain containing signals is typically just a

fraction of the dimension of the acquired hypercube. In short, TD_{target} is chosen for a desired resolution, and then only a part of it acquired, N, which defines a compression factor, N/TD_{target}. This situation of high sparsity suggested that a fraction of the points can be actually acquired, if proper algorithms exist that can reconstruct the frequency signal correctly. This field of research was propelled by the implementation of fast algorithms of the kind, which typically first reconstruct the full n-dimensional grid and then rely on FFT to produce the frequency domains.

The previous sections of this review have illustrated the typical layouts of MaxQ spectra of mixtures. For the most challenging cases, the signals cluster around dense areas, corresponding to fragments with very similar proton chemical shifts. Moreover, large spectral widths are required for accommodating the entirety of the MQ signals. These two conditions would impose large experimental times on useful MaxQ spectra, so that in this case acceleration by methods such as NUS can prove appealing. Indeed, clustering of signals in different regions of the spectrum assures the high sparsity condition that guarantees the success of compression. Also, it is a condition in which other methods that can enhance resolution, such as linear prediction (LP), have little impact, since this latter tries to reach its goal by using the information in the acquired points, TD, to extrapolate to the TD_{target}, a procedure that is likely to fail if these two quantities differs substantially. On the other hand, LP and NUS can be used in combination, as shown in Fig. 23.

The NUS approach was first tried on the same mixture as depicted in Fig. 13, for the 5Q correlation. This particular spectrum did not show insufficient resolution already with the classic (uniformly sampled, US) acquisition, with 256 points in the indirect dimension. Thus, in this case, NUS is not expected to achieve more than a cosmetic effect, similar to the one provided by LP, for instance, as demonstrated in the right panels of Fig. 23. On the other hand, the 3Q–1Q correlation spectrum is more dense in peaks (Fig. 24) and thus it can profit more from NUS. In this case reconstruction artifacts, at the time of the experiments reported, only one reconstruction method was available with commercial software, the recursive multidimensional decomposition (R-MDD) approach, which has since been complemented by the better performing compressed sensing algorithms, particularly the one based on iterative soft linear thresholding [58–60]. Indeed, the same data sets reprocessed with this latter approach presented negligible artifacts even for the 6.25% compression factor. In these conditions, high-order MQ spectra should probably always profit from the NUS option.

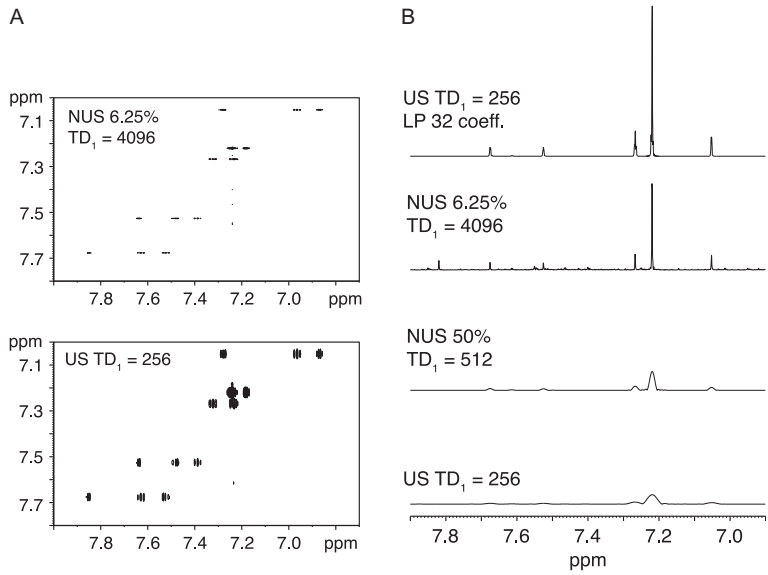

Figure 23 Demonstration of NUS sampling (with RMDD reconstruction, see text). The sample was a mixture of aromatic compounds similar to the one shown and discussed in Fig. 13. For this 5Q spectrum, the systems were, from top to bottom in the 5Q dimension, phenol, *o*-terphenyl, dibenzyl, acetanilide, and benzophenone. *Reproduced from Ref. [61] with permission from Elsevier.*

6. CONJUGATING MQ AND NMR DIFFUSOMETRY

NMR diffusometry is another common experiment used to characterize multicomponent samples [63–66], which has also been the objective of extensive reviewing [67]. PFGs are applied to label the molecular position, most typically along the main axis of the sample holder (a tube or a rotor). After sometime allowed for self-diffusion to operate random displacements, a second PFG is used to unwarp the position-dependent phase imparted on the signals. Molecules that did not change position will contribute coherently to the intensity of the signal after this process, having all zero phase distortion. Conversely, the rest of the sample will create destructive interference due to random phase distortions. Neglecting relaxation effects to the first order, the decay of the echo intensity as a function of the gradient intensity, G, relates, for isotropic media, to the diffusion coefficient, D

$$\exp\left[-Dp^2q^2(\Delta')\right] \tag{4}$$

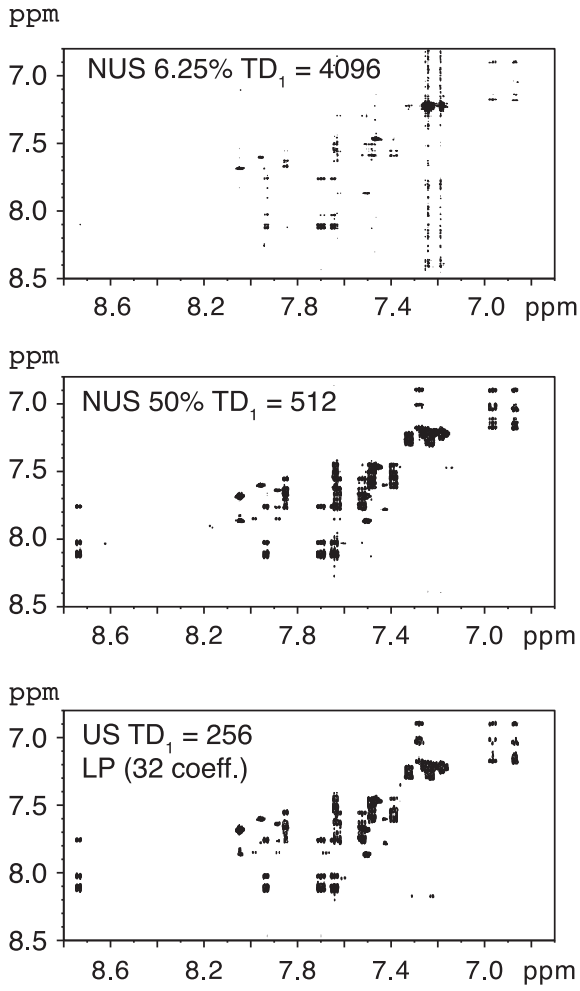

Figure 24 Comparison of 3Q–1Q correlation spectra recorded and processed with different US and NUS schemes. The sample was a mixture of aromatic compounds (phenol, *o*-terphenyl, dibenzyl, acetanilide, benzophenone, fluoranthene, naphthalene, anthracene, phenanthrene, triphenylene). *Reproduced from Ref. [61] with permission from Elsevier.*

where $q = \gamma G \delta$ (γ the gyromagnetic ratio and δ is gradient pulse duration) and Δ' is the diffusion delay corrected for gradient pulse duration and shape ($\Delta' = \Delta - \delta/3$ for a square gradient pulse, for instance).

In a first application of combined MQ and diffusometry to mixtures, Dalvit *et al.* [28] incorporated diffusion-editing during the pumping period, to allow measurement of the diffusion coefficients using a 2Q correlation

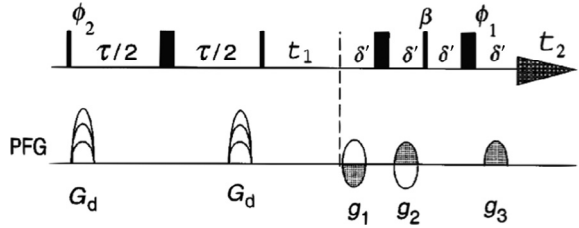

Figure 25 Pulse sequence for a diffusion-edited DQS as used in Ref. [28]. The gradients of variable intensity for encoding the diffusion decay are placed during the pumping period. The rest of the sequence is a common DQ correlation experiments, acquired with the echo/antiecho procedure for pure phase lineshapes. *Reproduced from Ref. [28] with permission from John Wiley and Sons.*

experiment (Fig. 25). The diffusion effects were encoded with $p=1$. An example of their result is illustrated in Fig. 26, where the decay of the intensity of a few cross-peaks from the 2Q spectrum as a function of the increasing gradient strength is shown. The authors were capable of determining this way the D values for the lighter molecules, but the analysis of VLDL and LDL proteins did not show any reliable result, as their MW falls outside the known range of accessible diffusion coefficients for standard solution state hardware (i.e., $>10^{-13}$ m^2 s^{-1}).

Equation (4) shows that, if the encoding–decoding of the molecular displacement takes place while a p-coherence order has been selected, the effect of the encoding gradient is multiplied by p, with a squared effect on the decay. This property was exploited early in the study of MQ-NMR, and it was first demonstrated on solutes in nematic solvents, as shown in Fig. 27 [68,69].

Furthermore, Norwood exploited the MaxQ coherence to counter the interferences due to the J couplings in the case of diffusometry using spin-echo experiments [70]. The approach proposed in that work was to use the pulse sequence in Fig. 28, in the presence of a field gradient of constant intensity, G.

In this case, the overall temporal evolution is:

$$I(\tau_1,\tau_2)=I(0)\exp\left[-2(\tau_1+\tau_2)/T_2-(2/3)\gamma^2n^2G^2D\left(\tau_1^3+\tau_2^3\right)\right] \quad (5)$$

In practice, a series of experiments are performed by varying τ_1, while keeping $(\tau_1+\tau_2)$ constant. Thus, the relaxation term becomes a simple multiplicative factor, and a plot of $\mathrm{Ln}(I(\tau_1,\tau_2)$ versus $\left(\tau_1^3+\tau_2^3\right)$ provides a linear decay allowing to determine D. This setup is perturbed, as all other NMR

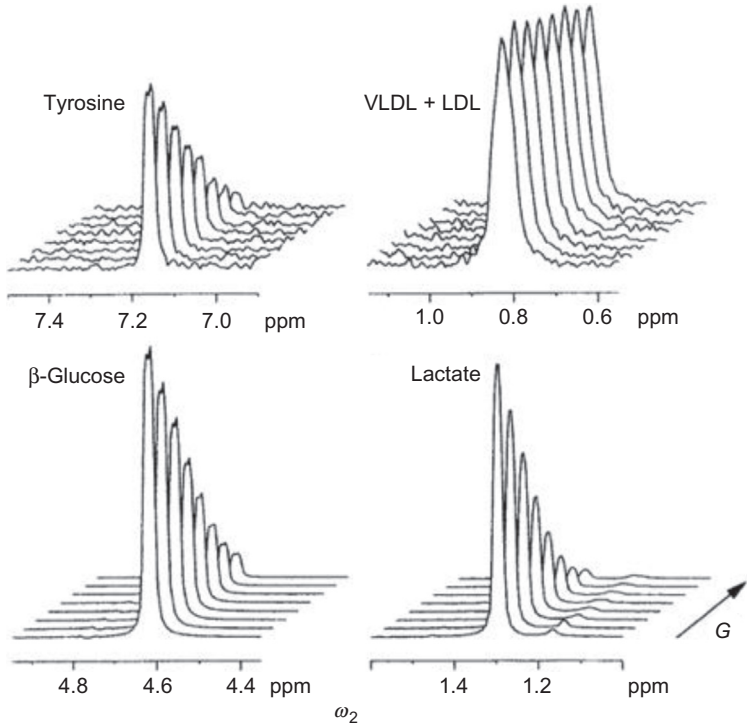

Figure 26 Pulse field gradient decays of DQ signals of cross-peaks from the 2Q spectrum as a function of the increasing gradient strength. *Reproduced from Ref. [28] with permission from John Wiley and Sons.*

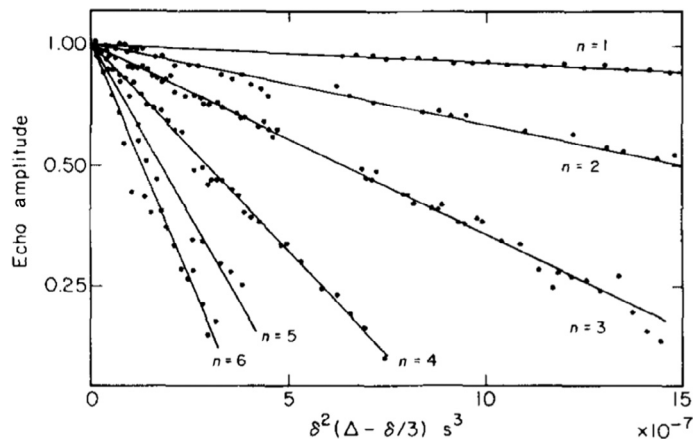

Figure 27 Demonstration of the dependence on the square of the coherence order (*n* in this plot) of the decay of a PFG experiment with variable. *Reproduced from Ref. [68] with permission from the American Institute of Physics.*

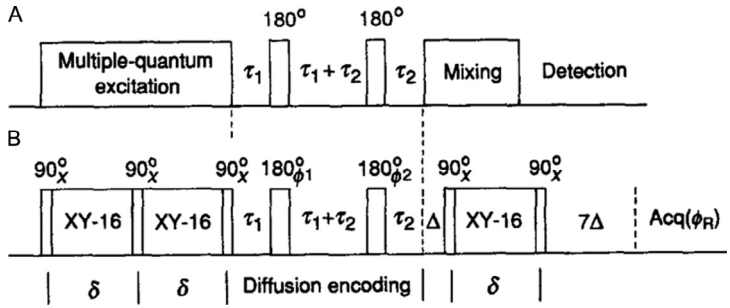

Figure 28 Pulse sequences for multiple-quantum diffusometry, in the presence of a gradient of magnetic field of constant intensity. The use of the XY-16 isotropic mixing was chosen to ameliorate the homogeneity of the MQ excitation. *Reproduced from Ref. [69] with permission from Elsevier.*

diffusometry sequences based on coherences (i.e., not on stimulated echoes in which the magnetization is stored along the z-axis during the diffusion time) by a common problem: oscillations of the decay due to the J couplings. Norwood recognized that the MaxQ coherence being unaffected by the coupling Hamiltonian, it could be best used to palliate to this problem. Indeed, experiments on the 7Q spectrum of 2-propanol were shown to possess excellent linearity, while the 1Q equivalent was badly affected by said oscillations (Fig. 29).

Since the advent of the DOSY displays [65,66], diffusometry has become even a more popular tool for the analysis of mixtures. This relies on the construction of a dimension [71–73], with the diffusion coefficient D (in units of $m^2\ s^{-1}$ or equivalent) as one of the axis. We shall refer to this experiment, one in which the diffusion is encoded on a p-quantum coherence, a pQDOSY. Inverse Laplace transform of Eq. (4), or an equivalent algorithm, is required to build the DOSY charts. If the observed decays stems from overlapping signals from more than one compound, the inversion requires the notoriously unstable problem of the inversion of a multiexponential decay. While many methods have been put forward to stabilize this calculation, best results are always obtained by reducing to a maximum the overlapping of the signals, so that MQF are certainly good candidates to integrate in a DOSY analysis.

A test case using MaxQDOSY, with $p=4$, for a sample comprising four aromatic molecules, is performed recently: anthracene, phenanthrene, naphthalene, and fluorene [74]. The system under scrutiny allowed $p=1$–4. The corresponding three 2D DOSYMQ along with the classic

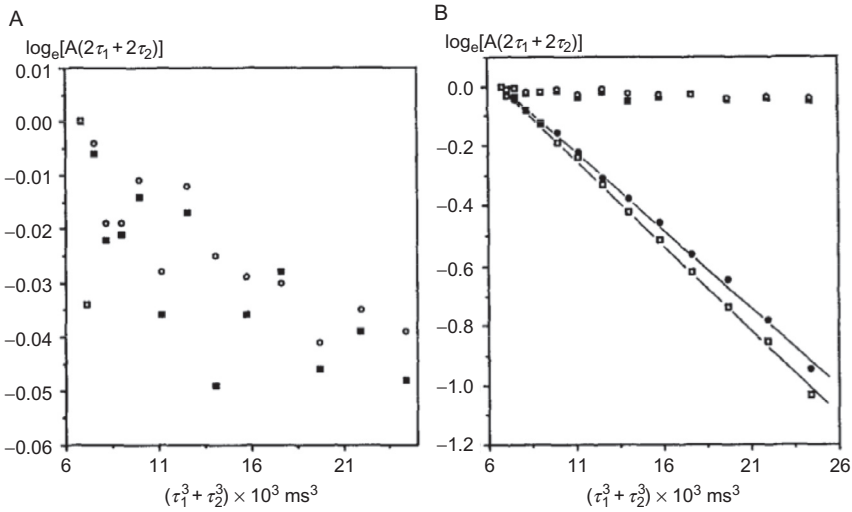

Figure 29 Effect of the MaxQ coherence on the behavior of diffusometry curves. Graphs of $\ln(A(2\tau_1+2\tau_2)]$ against $\left(\tau_1^3+\tau_2^3\right)$ for 5% and 10% solutions of 2-propanol in D_2O (see Eq. 5). Left: Single quantum CPTG experiment (see text for details), showing oscillation due to *J* couplings and impeding a proper analysis of the diffusion coefficient. Right: MaxQ ($p=7$) diffusion curves, showing suppression of the *J*-coupling oscillation; the 1Q curves are shown for comparison to highlight the dependence of the decay on p^2. *Reproduced from Ref. [69] with permission from Elsevier.*

DOSY experiments were unable to properly resolve the peaks belonging to the four compounds, although the $p=4$ layout almost correctly split the signal, with a noticeable exception being the peaks around 7.52 ppm. Going to higher p values had a simplifying effect, although a modest one, on the ^1H spectrum, with just the peaks belonging to the central ring of anthracene, bearing just two protons, disappearing.

Conversely, no ambiguity whatsoever is found in the case of the full 3D MaxQ experiment, a 4Q-4QDOSY correlation. Here, the projection along the three dimensions was all very well resolved, and the MaxQ correlation (dimensions 1 and 3) provides the expected separation quality. On the other hand, the 4QDOSY-1Q projection plane is also better resolved its 2D counterpart, with all peaks assigned to the correct spin system, without ambiguity. However, it is the 4Q-4QDOSY projection plan that presents the most spectacular resolution, with only one peak per molecule providing information on the molecular diffusivity (and thus roughly on its molecular volume) [73,75] and on the average chemical shift, δ_{MaxQ}. The impressive amelioration in resolution was probably arising as a consequence of the further spread

of the signal doing to the use of a third dimension and to the specific properties of the MaxQ coherences. This reduces the overlap when performing the DOSY transform. In short, the fact that the MaxQ dimension presents no overlap profits not only to the MaxQ-MaxQDOSY projection but also to the 1Q-MaxQDOSY one. Again, all the processing was performed within the Topspin software, and the much more sophisticated algorithms for the DOSY transform that has been demonstrated in the literature can further improve the analysis [75,76].

Finally, application of NUS allowed compressing of the recording time to very reasonable durations (here, about 35 min for concentrations of the order of 10 mM, not shown).

7. CONCLUSIONS

In summary, in what may look as yet one cycle of rediscovery, MQ-NMR is proving itself valuable in the analysis of complex mixtures of light molecules, such as metabolites. This is part of the extension of 2D techniques to mixture characterization, but it is also due to some specificity of the technique, namely the progressive simplification of the spectra by going to higher order and the very simple layout of MaxQ NMR, which carries some resemblance to DOSY, with a singlet correlating to the 1D ^{1}H spectrum of the coupled protons that originated it.

The main known limitations of the methods, namely the reduced sensitivity and the presence of peaks not arising from a direct coupling, have been shown to be affordable losses or even advantages for mixtures. Indeed, for the first issue, the technique can be compared to heteronuclear experiments, which are increasingly tested in the context of metabolomics for instance [55]. The "relay" peaks, signature of the presence of an extended spin coupling, can be even useful in the case of mixtures, as they facilitate the annotation of similar spin systems, much in the spirit of TOCSY.

REFERENCES

[1] M.H. Levitt, C. Radloff, R.R. Ernst, Coherence transfer selection rules induced by symmetry: application to NMR correlation spectroscopy, Chem. Phys. Lett. 114 (1985) 435–440.
[2] M. Munowitz, A. Pines, Principles and applications of multiple-quantum NMR, Adv. Chem. Phys. 66 (1987) 1–152.
[3] M.H. Levitt, R.R. Ernst, Multiple-quantum excitation and spin topology filtration in high-resolution NMR, J. Chem. Phys. 83 (1985) 3297–3310.
[4] G. Eich, G. Bodenhausen, R.R. Ernst, Exploring nuclear spin systems by relayed magnetization transfer, J. Am. Chem. Soc. 104 (1982) 3731–3732.

[5] G. Bodenhausen, Multiple-quantum NMR, Prog. Nucl. Magn. Reson. Spectrosc. 14 (1980) 137–173.
[6] T.J. Norwood, Multiple-quantum NMR methods, Prog. Nucl. Magn. Reson. Spectrosc. 24 (1992) 295–375.
[7] T.J. Norwood, Multiple quantum spectroscopy of liquid samples, in: D.M. Grant, R.K. Harris (Eds.), Encyclopedia of Magnetic Resonance, John Wiley & Sons, Chichester, 2007, pp. 3181–3188.
[8] N. Chandrakumar, 1D double quantum filter NMR studies, Annu. Rep. NMR. Spectrosc. 67 (2009) 265–329.
[9] C. Dalvit, M. Rance, P.E. Wright, Differentiation of direct and remote connectivities in phase-sensitive double-quantum spectra of proteins by variation of the multiple-quantum excitation period, J. Magn. Reson. 69 (1986) 356–361.
[10] M. Munowitz, A. Pines, Multiple-quantum nuclear-magnetic-resonance spectroscopy, Science 233 (1986) 525–531.
[11] A. Wokaun, R.R. Ernst, Multiple quantum double resonance, Mol. Phys. 36 (1978) 317.
[12] W.S. Warren, A. Pines, Simple pulse sequences for selective multiple-quantum excitation, Chem. Phys. Lett. 88 (1982) 441–443.
[13] J.B. Murdoch, W.S. Warren, D.P. Weitekamp, A. Pines, Computer simulations of multiple-quantum NMR experiments. I. Nonselective excitation, J. Magn. Reson. 60 (1984) 205.
[14] G.N. Manjunatha Reddy, S. Caldarelli, Demixing of severely overlapping NMR spectra through multiple quantum NMR, Anal. Chem. 82 (8) (2010) 3266–3269.
[15] G.N. Manjunatha Reddy, S. Caldarelli, Maximum-quantum (MaxQ) NMR for the speciation of mixtures of phenolic molecules, Chem. Commun. 47 (2011) 4297–4299.
[16] G.N. Manjunatha Reddya, S. Caldarelli, Identification and quantification of EPA 16 priority polycyclic aromatic hydrocarbon pollutants by maximum-quantum NMR, Analyst 137 (2012) 741–746.
[17] S. Sinton, A. Pines, Study of liquid-crystal conformation by multiple quantum NMR—normal-pentyl cyanobiphenyl, Chem. Phys. Lett. 76 (1980) 263–267.
[18] R.R. Ernst, G. Bodenhausen, A. Wokaun, Principles of Nuclear Magnetic Resonance in One and Two Dimensions, Clarendon Press, Oxford, UK, 1990.
[19] G.N. Manjunatha Reddy, S. Caldarelli, Improved excitation uniformity in multiple-quantum NMR experiments of mixtures, Magn. Reson. Chem. 51 (2013) 240–244.
[20] C. Balo, F. Fernandez, C. Gonzalez, C. Lopez, ^{1}H NMR spectra of monosubstituted phenanthrenes, Spectrochim. Acta A 50 (1994) 937.
[21] W.S. Warren, S. Sinton, D.P. Weitekamp, A. Pines, Selective excitation of multiple-quantum coherence in nuclear magnetic-resonance, Phys. Rev. Lett. 43 (1979) 1791–1794.
[22] L. Braunschweiler, G. Bodenhausen, R.R. Ernst, Analysis of networks of coupled spins by multiple quantum N.M.R., Mol. Phys. 48 (1983) 535–560.
[23] C. Dalvit, J.M. Bohlen, Proton phase-sensitive pulsed field gradient double-quantum spectroscopy, Annu. Rep. NMR. Spectrosc. 37 (1999) 203–271.
[24] D.P. Weitekamp, J.R. Garbow, J.B. Murdoch, A. Pines, High-resolution NMR-spectra in inhomogeneous magnetic-fields—application of total spin coherence transfer echoes, J. Am. Chem. Soc. 103 (1981) 3578–3579.
[25] J.R. Garbow, D.P. Weitekamp, A. Pines, Total spin coherence transfer echo spectroscopy, J. Chem. Phys. 79 (1983) 5301.
[26] C. Zhong, C. Zhiwei, J. Zhong, High-resolution NMR spectra in inhomogeneous fields via IDEAL (intermolecular dipolar-interaction enhanced all lines) method, J. Am. Chem. Soc. 126 (2004) 446–447.
[27] C. Honghao, C. Yushan, C. Xiaohong, C. Shuhui, C. Zhong, High-resolution 1H NMR spectroscopy of fish muscle, eggs and small whole fish via Hadamard-encoded intermolecular multiple-quantum coherence, PLoS One 9 (2014). e86422.

[28] C. Dalvit, J.M. Böhlen, Analysis of biofluids and chemical mixtures in non-deuterated solvents with 1H diffusion-weighted PFG phase-sensitive double-quantum NMR spectroscopy, NMR Biomed. 10 (1997) 285–291.
[29] E. Martineau, I. Tea, S. Akoka, P. Giraudeau, Absolute quantification of metabolites in breast cancer cell extracts by quantitative 2D 1H INADEQUATE NMR, NMR Biomed. 25 (2012) 985–992.
[30] B. Baishya, N. Suryaprakash, Spin selective multiple quantum NMR for spectral simplification, determination of relative signs, and magnitudes of scalar couplings by spin state selection, J. Chem. Phys. 127 (2007) 214510.
[31] F. Shahidi, P.K. Janitha, P.D. Wanasundara, Phenolic antioxidants, Crit. Rev. Food Sci. Nutr. 32 (1992) 67–103.
[32] L. Cinquanta, M. Esti, M.D. Matteo, Oxidative stability of virgin olive oils, J. Am. Oil Chem. Soc. 78 (2001) 1197–1202.
[33] M. Tsimidou, Polyphenols and quality of virgin olive oil in retrospect, Ital. J. Food Sci. 10 (1998) 99–116.
[34] M. Esti, L. Cinquanta, E.L. Notte, Phenolic compounds in different olive varieties, J. Agric. Food Chem. 46 (1998) 23–35.
[35] M. Brenes, A. Garcia, P. Garcia, J.J. Rios, A. Garrido, Phenolic compounds in Spanish olive oils, J. Agric. Food Chem. 47 (1999) 3535–3540.
[36] E.N. Frankel, Chemistry of extra virgin olive oil: adulteration, oxidative stability, and antioxidants, J. Agric. Food Chem. 58 (2010) 5991–6006.
[37] D.M.A.M. Luykx, R.J.B. Peters, S.M.V. Ruth, H. Bouwmeester, A review of analytical methods for the identification and characterization of nano delivery systems in food, J. Agric. Food Chem. 56 (2008) 8231–8247.
[38] R.J. McGorrin, One hundred years of progress in food analysis, J. Agric. Food Chem. 57 (2009) 8076–8088.
[39] V. Rizzo, V. Pinciroli, Quantitative NMR in synthetic and combinatorial chemistry, J. Pharm. Biomed. Anal. 38 (2005) 851–857.
[40] S. Sanchez, F. Ziarelli, S. Viel, C. Delaurent, S. Caldarelli, Improved solid-state NMR quantifications of active principles in pharmaceutical formulations, J. Pharm. Biomed. Anal. 47 (2008) 683–687.
[41] K. Bingol, R. Bruschweiler, Multidimensional approaches to NMR-based metabolomics, Anal. Chem. 86 (2014) 47–57.
[42] I.A. Lewis, S.C. Schommer, B. Hodis, K.A. Robb, M. Tonelli, W.M. Westler, M.R. Sussman, J.L. Markley, Method for determining molar concentrations of metabolites in complex solutions from two-dimensional ^{1}H-^{13}C NMR spectra, Anal. Chem. 79 (2007) 9385–9390.
[43] F. Hu, K. Furihata, Y. Kato, M. Tanokura, Nondestructive quantification of organic compounds in whole milk without pretreatment by two-dimensional NMR spectroscopy, J. Agric. Food Chem. 55 (2007) 4307–4311.
[44] N. Shanaiah, M.A. Desilva, G.A.N. Gowda, M.A. Raftery, B.E. Hainline, D. Raftery, Class selection of amino acid metabolites in body fluids using chemical derivatization and their enhanced ^{13}C NMR, Proc. Natl. Acad. Sci. U.S.A. 104 (2007) 11540–11544.
[45] F. Malz, H. Jancke, Validation of quantitative NMR, J. Pharm. Biomed. Anal. 38 (2005) 813–823.
[46] P. Schanda, Fast-pulsing longitudinal relaxation optimized techniques: enriching the toolbox of fast biomolecular NMR spectroscopy, Prog. Nucl. Magn. Reson. Spectrosc. 55 (2009) 238–265.
[47] E. Kupce, R.J. Freeman, Two-dimensional Hadamard spectroscopy, J. Magn. Reson. 162 (2003) 300–310.
[48] E. Kupce, R.J. Freeman, Projection–reconstruction technique for speeding up multidimensional NMR spectroscopy, J. Am. Chem. Soc. 126 (2004) 6429–6440.

[49] A. Tal, L. Frydman, Single-scan multidimensional magnetic resonance, Prog. Nucl. Magn. Reson. Spectrosc. 57 (2010) 241–292.
[50] A. Le Guennec, P. Giraudeau, S. Caldarelli, J.N. Dumez, Ultrafast double-quantum NMR spectroscopy, Chem. Commun. 51 (2015) 354–357.
[51] A. Le Guennec, P. Giraudeau, S. Caldarelli, Evaluation of fast 2D NMR for metabolomics, Anal. Chem. 86 (2014) 5946–5954.
[52] P. Giraudeau, S. Massou, Y. Robin, E. Cahoreau, J.C. Portais, S. Akoka, Ultrafast quantitative 2D NMR: an efficient tool for the measurement of specific isotopic enrichments in complex biological mixtures, Anal. Chem. 83 (2011) 3112–3119.
[53] D.L. Turner, Carbon-13 autocorrelation NMR using double-quantum coherence, J. Magn. Reson. 49 (1982) 175.
[54] A. Banerjee, N. Chandrakumar, Ultrafast homonuclear correlation spectroscopy with diagonal suppression, J. Chem. Phys. 140 (2014) 31103.
[55] M. Pathan, S. Akoka, I. Tea, B. Charrier, P. Giraudeau, "Multi-scan single shot" quantitative 2D NMR: a valuable alternative to fast conventional quantitative 2D NMR, Analyst 136 (2011) 3157–3163.
[56] A. Le Guennec, I. Tea, I. Antheaume, E. Martineau, B. Charrier, M. Pathan, S. Akoka, P. Giraudeau, Fast determination of absolute metabolite concentrations by spatially encoded 2D NMR: application to breast cancer cell extracts, Anal. Chem. 84 (2012) 10831–10837.
[57] M. André, M. Piotto, S. Caldarelli, J.-N. Dumez, Ultrafast high-resolution magic-angle-spinning NMR spectroscopy, Analyst 140 (2015) 3942–3946.
[58] M. Gal, C. Melian, D.E. Demco, B. Bluemich, L. Frydman, Solid-state single-scan 2D NMR under magic-angle-spinning, Chem. Phys. Lett. 459 (2008) 188–193.
[59] K. Kazimierczuk, J. Stanek, A. Zawadzka-Kazimierczuk, W. Kozminski, Random sampling in multidimensional NMR spectroscopy, Prog. Nucl. Magn. Reson. Spectrosc. 57 (2010) 420–434.
[60] V.Y. Orekhov, V.A. Jaravine, Analysis of non-uniformly sampled spectra with multi-dimensional decomposition, Prog. Nucl. Magn. Reson. Spectrosc. 59 (2011) 271–292.
[61] M. Piotto, G.N. Manjunatha Reddy, S. Caldarelli, Non-uniformly sampled maximum quantum spectroscopy, J. Magn. Reson. 213 (2011) 107–111.
[62] V. Jaravine, I. Ibraghimov, V.Y. Orekhov, Removal of a time barrier for high-resolution multidimensional NMR spectroscopy, Nat. Methods 3 (2006) 605–607.
[63] B. Antalek, Using pulsed gradient spin echo NMR for chemical mixture analysis: how to obtain optimum results, Concepts Magn. Reson. 14 (2002) 225–258.
[64] K.F. Morris, P. Stilbs, C.S. Johnson Jr., Analysis of mixtures based on molecular size and hydrophobicity by means of diffusion-ordered 2D NMR, Anal. Chem. 66 (1994) 211–215.
[65] P. Stilbs, Fourier transform pulsed-gradient spin-echo studies of molecular diffusion, Prog. Nucl. Magn. Reson. Spectrosc. 19 (1987) 1–45.
[66] H. Barjat, G.A. Morris, S. Smart, A.G. Swanson, S.C.R. Williams, High-resolution diffusion-ordered 2D spectroscopy (HR-DOSY)—a new tool for the analysis of complex mixtures, J. Magn. Reson. B 108 (1995) 170–172.
[67] K.F. Morris, C.S. Johnson Jr., Diffusion-ordered two-dimensional nuclear magnetic resonance spectroscopy, J. Am. Chem. Soc. 114 (1992) 3139–3141.
[68] D. Zax, A. Pines, Study of anisotropic diffusion of oriented molecules by multiple quantum spin echoes, J. Chem. Phys. 78 (1983) 6333–6334.
[69] J.F. Martin, L.S. Selwyn, R.R. Vold, R.L. Vold, The determination of translational diffusion constants in liquid crystals from pulsed field gradient double quantum spin echo decays, J. Chem. Phys. 76 (1982) 2632.
[70] T.J. Norwood, An Eddy-current-independent multiple-quantum method for measuring the diffusion of coupled spins, J. Magn. Reson. 99 (1992) 208–213.

[71] S. Viel, S. Caldarelli, Improved 3D DOSY-TOCSY experiment for mixture analysis, Chem. Commun. (2008) 2013–2015.
[72] C.S. Johnson Jr., Diffusion ordered nuclear magnetic resonance spectroscopy: principles and applications, Prog. Nucl. Magn. Reson. Spectrosc. 34 (1999) 203–256.
[73] G.A. Morris, Diffusion-ordered spectroscopy, in: R.K. Harris, R.E. Wasylishen (Eds.), Encyclopedia of Magnetic Resonance, Wiley, Chichester, 2009. http://dx.doi.org/10.1002/9780470034590.emrstm0119.pub2.
[74] M. Yemloul, G.N. Manjunatha Reddy, S. Caldarelli, manuscript in preparation.
[75] R. Evans, Z. Deng, A.K. Rogerson, A.S. McLachlan, J.J. Richards, M. Nilsson, G.A. Morris, Quantitative interpretation of diffusion-ordered NMR spectra: can we rationalize small molecule diffusion coefficients? Angew. Chem. Int. Ed. Engl. 52 (2013) 3199–3202.
[76] M. Nilsson, The DOSY Toolbox: a new tool for processing PFG NMR diffusion data, J. Magn. Reson. 200 (2009) 296–302.